*Korean J. Chem. Eng.*, 34(1), 81-86 (2017)
DOI: 10.1007/s11814-016-0239-7

pISSN: 0256-1115
eISSN: 1975-7220

# Effect of acid treatment of Fe-BEA zeolite on catalytic $N_2O$ conversion

**Jeong Min Jeong*, Ji Hye Park*, Jeong Hun Baek*, Ra Hyun Hwang*, Sang Goo Jeon**, and Kwang Bok Yi***,†**

*Graduate School of Energy Science and Technology, Chungnam National University, 99 Daehak-ro, Yuseong-gu, Daejeon 34134, Korea
**Bio Resource Cycling Laboratory, Korea Institute of Energy Research, 152 Gajeong-ro, Yuseong-gu, Daejeon 34129, Korea
***Department of Chemical Engineering Education, Chungnam National University, 99 Daehak-ro, Yuseong-gu, Daejeon 34134, Korea
(*Received 24 May 2016 • accepted 19 August 2016*)

**Abstract**−The effect of acid treatment on the physical and chemical characteristics of BEA zeolite, as well as the catalytic activity of the Fe-BEA catalyst for $N_2O$ reduction under $NH_3$-selective catalytic reduction ($NH_3$-SCR) conditions, was examined. The acid treatment caused dealumination of BEA and enrichment of the silanol groups on vacant T-sites and the Brønsted acid sites. As the acid treatment time increased, the silanol groups and the weak acid sites in BEA also increased. Because the weak acid sites behave as anchoring sites for Fe ions, the catalytic activity also increased as the treatment time increased. However, extended exposure of BEA to acid decreased the catalytic activity of the Fe-BEA catalyst somewhat, and decreased the silanol groups and weak acid sites. The catalytic activity and the amount of weak acid sites were well correlated with the BEA acid treatment time.

Keywords: $N_2O$ Reduction, Fe-BEA, $NH_3$-SCR, Acid Treatment, Dealumination

## INTRODUCTION

Since the Kyoto protocol was announced, $N_2O$, like $CO_2$, has been considered a major greenhouse gas. Even though emissions of $N_2O$ are relatively small, $N_2O$ has a great impact on global warming because its global warming potential (GWP) is 310 times that of $CO_2$ [1-3]. Catalytic thermal decomposition [4-10] and selective catalytic reduction (SCR) with reductants such as ammonia [11,12] have been proposed and implemented as technologies to reduce $N_2O$ emissions. Of these, SCR of $N_2O$ with ammonia has recently gained more attention because its energy consumption requirements are less intensive than those of catalytic thermal decomposition [13-17].

Zeolites are widely used in various industrial catalytic applications for their stability, activity, and high selectivity [18-21]. Metal-containing zeolites were found to be efficient catalysts for $N_2O$ decomposition, as well as for the SCR of $N_2O$ with ammonia [22-26]. Mauvezin et al. studied $N_2O$ reduction by ammonia with various types of zeolites, such as BEA, MFI, FAU, and FER, and found that Fe ion-exchanged BEA and FER zeolites were the most promising catalysts for $N_2O$ reduction [27]. Kamasamudram et al. compared Fe- and Cu-containing zeolites, and found that Fe-containing zeolites have higher activities as catalysts for $N_2O$ reduction [28]. Øygarden and Pérez-Ramírez compared various modified zeolites containing Fe and reported that dealuminated BEA had the highest catalytic activity for $N_2O$ reduction [29].

Zeolite modification to tune catalytic properties is often performed by dealumination. Steam and/or acid treatment usually lead to partial dealumination of zeolites, resulting in particular acidic properties and catalytic activities of the zeolites [30-34]. Although it has been proposed that an appropriate dealumination process would improve the catalytic activities of metal-supported zeolite, however the effect of dealumination by acid treatment on the catalytic activity of Fe-BEA has not been reported.

In this study, we investigated the physical and chemical properties, as well as the catalytic activities, of Fe-BEA catalysts that were prepared by dealumination of BEA zeolites by nitric acid with various treatment times.

## EXPERIMENTAL

### 1. Catalyst Preparation

BEA zeolite (Zeolyst, CP814E, $SiO_2/Al_2O_3$=25) was treated with 0.2 M $HNO_3$ solution for varying treatment times (10, 30, and 60 min). Then, the acid-treated BEA was washed with distilled water and put in an aqueous solution containing 0.004 M of $Fe(NO_3)_3 \cdot 9H_2O$ (Sigma Aldrich, 98%). The resulting solution was stirred for 15 h before filtration. The filter cake was dried overnight in a convection oven at 373 K. This procedure was repeated three times, and then the ion-exchanged BEA was calcined in air at 773 K for 6 h. The prepared catalysts were designated according to the acid treatment time as Fe-BEA(10), Fe-BEA(30), and Fe-BEA(60). For instance, Fe-BEA(10) is the catalyst prepared via Fe ion-exchange of BEA that was pretreated with acid for 10 min.

### 2. $N_2O$ Reduction by $NH_3$-SCR

$NH_3$-selective catalytic reduction ($NH_3$-SCR) was carried out in

†To whom correspondence should be addressed.
E-mail: cosy32@cnu.ac.kr

a fixed bed reactor in the temperature range of 623-673 K. The prepared catalyst was sieved to achieve a particle diameter range of 250-355 μm. Approximately 400 mg of sieved catalyst was placed in the reactor, and reactor temperature was increased from room temperature to 623 K for 95 min for heat treatment. Then, the temperature was decreased to 573 K before the reactant gas mixture was injected. The reactant gas mixture consisted of 300 ppm $NO_X$, 300 ppm $N_2O$, 600 ppm $NH_3$, 3 vol% $O_2$, and balance $N_2$. The flow rate of the gas mixture was controlled by a mass flow controller (MFC, Brooks), and the gas hourly space velocity (GHSV) was 45,000 $h^{-1}$. Then, the reactor was heated to 673 K at intervals of 10 K. The $N_2O$ concentration in the effluent gas was measured using an on-line gas analyzer (Siemens Ultramat 6).

**3. Catalyst Characterization**

The compositions of all the samples were determined by an inductively coupled plasma atomic emission spectrometer (ICP-AES, OPTIMA 7300 DV, Perkin-Elmer).

The surface morphology of the catalyst was investigated by using field emission-scanning electron microscopy (FE-SEM, S-4800, Hitachi). The BET surface area was measured with $N_2$ at 77 K using a Micromeritrics model ASAP 2010 instrument following pretreatment of the samples at 473 K for 4 h.

The acid site concentration was measured by $^{27}Al$ and $^{1}H$ magic-angle-spinning (MAS) NMR (500 MHz, Varian Unity INOVA). All solid-state MAS NMR measurements were on a Varian INOVA spectrometer at a rotating frequency of 15 kHz at 298 K. The Al spectra were recorded at a resonance frequency of 130.3 MHz with 4000 scans. The excitation pulse length was 1.0 μs, and the recycle time was 1.0 s. The chemical shifts were referenced to an external standard ($Al(NO)_3$, $\delta$=0.54 ppm). The spectra were normalized to the sample mass for quantitative comparison. For $^{1}H$ MAS NMR, the spectra were recorded at a resonance frequency of 499.9 MHz with 800 scans. The pulse length and the recycle time were 4.0 μs and 5 s, respectively. Tetramethysilane (TMS) was used as a reference.

$NH_3$-TPD (temperature-programmed desorption, BELCAT-M, Bel Japan) was used to measure the acid strength and relative amount of acid. The sample cell was heated at a rate of 10 K/min to 523 K under a flow of He (50 ml/min). When the thermal conductivity detector (TCD) was stabilized at 523 K, the sample cell was cooled to 373 K. Then, $NH_3$ gas was flowed through the sample cell for 30 min, and the cell was flushed with He until $NH_3$ was not detected. Finally, the sample cell was heated at a rate of 5 K/min to 873 K, while desorbed $NH_3$ was measured with the TCD. In situ diffuse reflectance infrared Fourier transform spectroscopy (DRIFTS, Nicolet iS10, Thermo Scientific) was used to investigate structural changes in the acid-treated catalysts as the reactant gas was introduced. Spectra were recorded at 4 $cm^{-1}$ resolution with 64 scans in a cell equipped with ZnSe windows. All samples were heat treated for 30 min at 773 K in a $N_2$ atmosphere before measurement. The spectrum of KBr was used as a reference for all measurements.

## RESULTS AND DISCUSSION

**1. Physicochemical Characterization of Fe-BEA**

The prepared Fe-BEA catalysts and BEA zeolite were character-

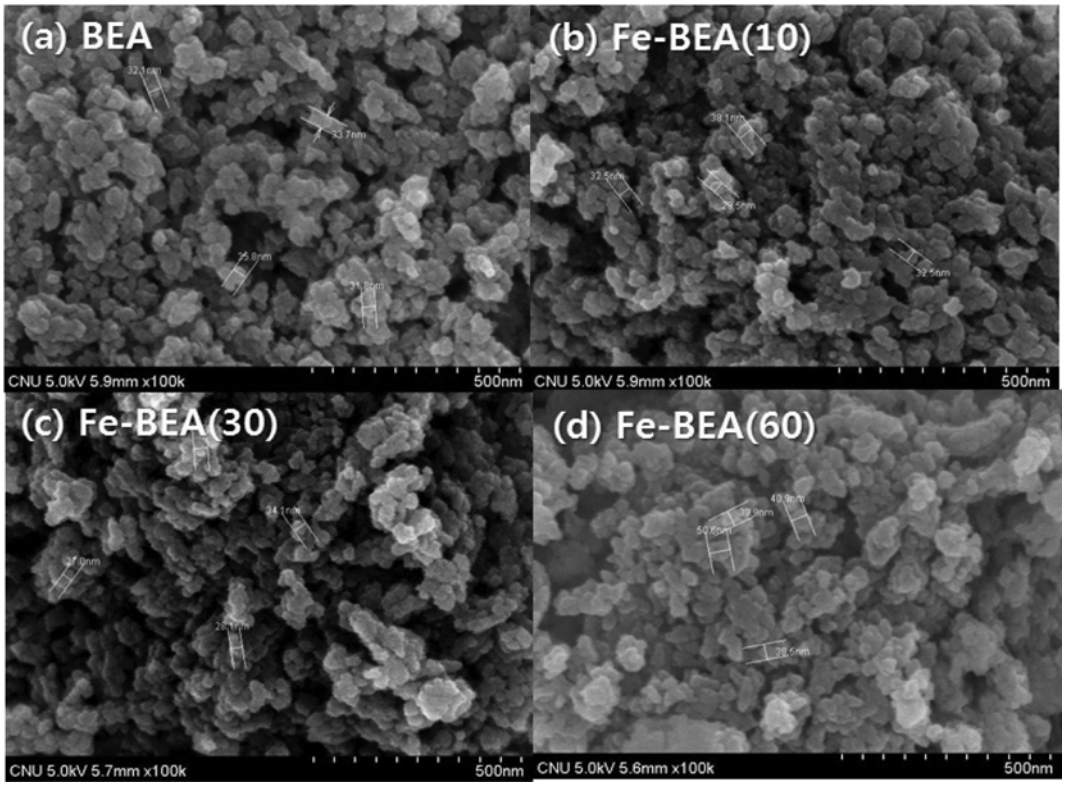


**Fig. 1. SEM images of (a) BEA and Fe-BEA zeolite catalysts treated with acid for (b) 10, (c) 30, and (d) 60 min.**

**Table 1. Composition of acid-treated zeolite catalysts. (analyzed by ICP-AES)**

| Catalyst | $HNO_3$ (0.2 M) treatment time, min | Fe [wt%] | Al [wt%] | Si [wt%] | Bulk molar ratio (Fe/Al) |
|---|---|---|---|---|---|
| BEA zeolite | - | - | 1.75 | 29.0 | - |
| Fe-BEA(10) | 0.2 M/10 min | 2.72 | 0.86 | 30.3 | 1.52 |
| Fe-BEA(30) | 0.2 M/30 min | 2.33 | 0.25 | 27.9 | 4.50 |
| Fe-BEA(60) | 0.2 M/60 min | 2.03 | 0.26 | 32.0 | 3.86 |

ized prior to the catalytic activity test. Fig. 1 shows SEM images of the catalysts. All the samples appeared to consist of particles with sizes in the range of 40-50 nm with similar particle shapes. Neither the acid treatment nor the Fe ion-exchange process affected the apparent morphology of the catalyst surface. The concentrations of Al and Fe in BEA and Fe-BEA catalysts were measured by ICP-AES; their values are shown in Table 1. As expected, the concentration of Al decreased with the acid treatment. Al concentration in BEA was measured as 1.75 wt% and decreased to 0.86, 0.25 and 0.26 wt% after 10, 30, and 60 min of acid treatment, respectively. The Fe loadings in Fe-BEA appeared to decrease from 2.72 to 2.06 wt% as the acid treatment time increased. This indicates that the not all Fe ions take positions on the vacant sites from which Al atoms are removed. The surface areas, pore volumes, and pore diameters determined by BET analysis were very similar for all samples (Table 2). Although the acid treatment and Fe ion-exchange process seemed to increase pore volume and pore diameter slightly, the change was too small to be significant.

**Table 2. BET analysis results for acid-treated zeolite catalysts**

| Catalyst | $S_{BET}$ ($m^2$/g) | Pore volume ($cm^3$/g) | Pore diameter (Å) |
|---|---|---|---|
| BEA zeolite | 633 | 0.75 | 48 |
| Fe-BEA(10) | 644 | 0.83 | 52 |
| Fe-BEA(30) | 679 | 0.84 | 50 |
| Fe-zeolite(60) | 625 | 0.84 | 54 |

**2. Changes in Environment of Al Species During Acid Treatment**

The local structural changes of Al T-atoms were characterized by $^{27}$Al MAS NMR spectroscopy. In the NMR spectra shown in Fig. 2, signals assigned to tetrahedral Al species were observed between 50 and 65 ppm in addition to resonances corresponding to extra-framework octahedral Al species around 20 ppm. The strong signal at 57 ppm in the BEA spectrum indicates the presence of tetrahedrally coordinated framework aluminum. The broad signal shape indicates two types of sites (T1-T2 at 54 ppm and T3-T9 at 57 ppm) [35]. The signal between 0 and 20 ppm represents extra-framework octahedral Al species. The broad shape of this signal suggests that the extra-framework octahedral species are in a rather distorted form, not a well-ordered form. After the acid treatment and Fe ion-exchange process, the tetrahedrally coordinated Al species clearly disappeared, and the signals of the octahedrally coordinated Al species sharpened. This change might indicate that the octahedrally coordinated Al species were transformed to a more ordered from. The dealumination process has been reported to produce vacant T-sites that can be used as anchoring points for metal ions following an ion-exchange process [34]. Therefore, it was assumed that the tetrahedrally coordinated Al species were removed during the acid treatment to produce empty T3-T9 sites and Fe ions were attracted to these empty sites during the subsequent ion-exchange process.

**3. Influence of Acid Treatment on Zeolite Acidity**

Fig. 3 shows the $^1$H MAS NMR spectra of BEA and the acid-treated Fe-BEA catalysts. $^1$H MAS NMR is useful for identifying

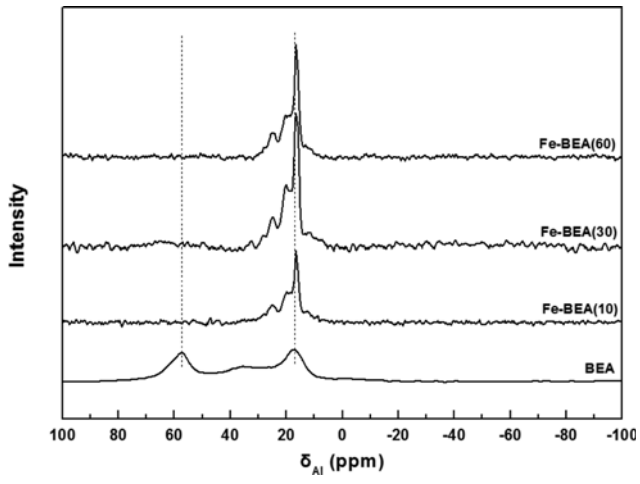


**Fig. 2. 1D $^{27}$Al MAS NMR spectra of BEA and acid-treated Fe-BEA catalysts.**

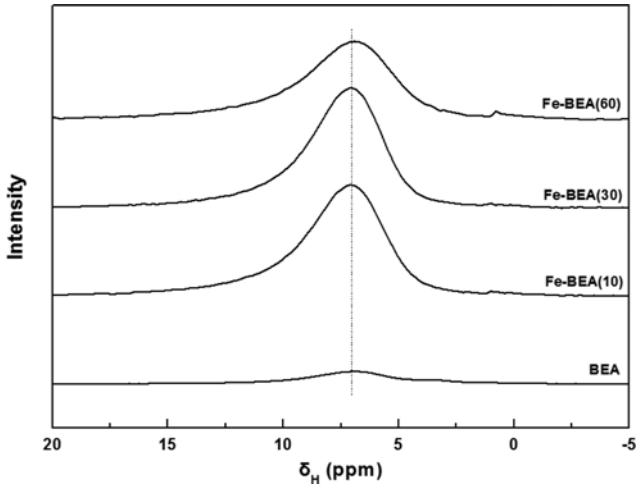


**Fig. 3. $^1$H MAS NMR spectra of BEA and acid-treated Fe-BEA catalysts.**

the hydroxyl groups in zeolites and measuring the Brønsted acidity. The signal assigned to the protons of a bridged Si-O(H)-Al Brønsted acid site was observed at 6.89 ppm for all samples. The signal was very weak, but its intensity increased significantly after the acid treatment and ion-exchange process. The intensities of the signal are in the order: Fe-BEA(30)>Fe-BEA(10)>Fe-BEA(60)>>BEA. The acid treatment is believed to remove alumina from the lattice and add more hydroxyl groups at the resulting empty site, and there are a few literature reports of similar phenomena [35,36]. The signal at 6.89 ppm is associated with silanol groups at vacant T-sites that are generated by acid treatment of zeolites [36]. Therefore, it is reasonable to consider that the intensity of this signal is proportional to the amount of hydrogen-bonded silanol groups at vacant T-sites that were created by the acid treatment. If these hydrogen-bonded silanol groups behave as anchoring sites for metal ions, the samples with higher intensities might have higher catalytic activities due to a higher density of Fe ions.

To investigate the effect of the acid treatment on the acidity of the catalysts, TPD tests were carried out. In the $NH_3$-TPD results shown in Fig. 4, two major peaks are observed for all samples with very similar shapes. The first and second peaks appeared in the temperature ranges of 443-463 K and 643-653 K, respectively. The first peak is attributed to desorption of $NH_3$ from weak Brønsted acid sites, whereas the second peak is attributed to desorption from Lewis acid sites [37]. The acid treatment appears to produce more weak acid sites. Although the maximum of the peaks varied somewhat with acid treatment time, the narrow temperature window indicates that the acid treatment time does not affect the acid strength. However, the number of acid sites was affected by the treatment time. As shown in Table 3, the total number of sites are in the order: Fe-BEA(30)>Fe-BEA (60)~Fe-BEA (10). The parent BEA apparently contains much higher concentration of total acid sites than Fe-BEA catalysts. The significant decrease of strong acid site concentration after Fe loading indicates that the most of Fe ions are bound to strong acid sites during the ion exchange step. The same phenomenon was witnessed when the Fe ions were loaded on BEA without the acid treatment in our previous experiment. When only Fe-BEA catalysts were concerned, however, it appears that moderate acid treatment resulted in increased the number of acid sites in Fe-BEA catalyst, but excessive treatment decreased the number of acid sites. Note that the change in total acid sites was mostly attributed to changes in the number of weak acid sites of Fe-BEA catalyst, as the number of strong acid sites only increased slightly with the treatment time. Thus, the acid treatment time only affected the weak acid sites. This result is consistent with $^1$H MAS NMR analysis. It is assumed that the nitric acid treatment removes Al from the lattice of the catalyst, resulting in production of vacant T-sites, in which silanol groups behave as anchoring sites for Fe ions. However, excessive acid treatment is believed to cause partial collapse of the zeolite structure through the formation of an amorphous phase [37-39]. Such a structural change could also cause some of the silanol groups and weak acid sites in the catalyst to collapse, resulting in decreased catalytic activity.

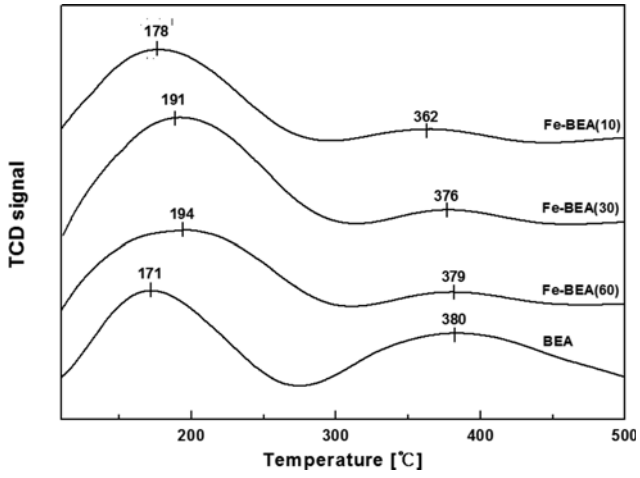


**Fig. 4. $NH_3$-TPD patterns for acid-treated Fe-BEA catalysts.**

**Table 3. Concentration of acid sites (mmol/g) in Fe-BEA catalysts with different acid treatment time**

| Catalyst | Total acid sites | Weak acid sites | Strong acid sites |
|---|---|---|---|
| BEA | 0.613 | 0.336 | 0.277 |
| Fe-BEA(10) | 0.404 | 0.372 | 0.032 |
| Fe-BEA(30) | 0.490 | 0.454 | 0.036 |
| Fe-BEA(60) | 0.390 | 0.352 | 0.038 |

**4. Effect of Acid Treatment on Zeolite Functional Groups**

Fig. 5 shows the IR spectra of the acid-treated Fe-BEA zeolites at 623 K in a $N_2$ atmosphere. In the region above 3,000 $cm^{-1}$, three major bands are observed at 3,739, 3,674, and 3,596 $cm^{-1}$. The band at 3,739 $cm^{-1}$ is assigned to terminal Si-OH groups, whereas that at 3,674 $cm^{-1}$ is associated with OH groups bonded to $Fe^{III}$ species. The band at 3,596 $cm^{-1}$ is attributed to the isolated bridging proton between Si(OH)Al and AlOH. These three bands were well observed in all Fe-BEA catalysts. However, the band at 3,674 $cm^{-1}$ was not observed in BEA. Furthermore, it is notable that the band at 3,596 $cm^{-1}$ was diminished when Fe was loaded. This indicates that all the three Fe-BEA catalysts were successfully loaded with Fe. The broad massif is reported to be due to interactions between SiOH and Si(OH)Al groups at defect sites [37]. As the intensities

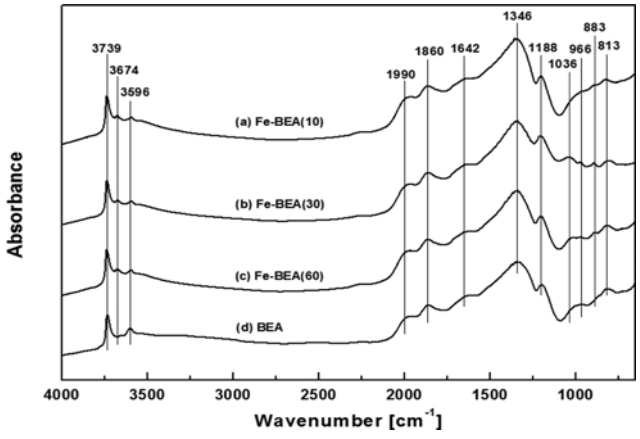


**Fig. 5. FTIR spectra of acid-treated Fe-BEA catalysts at 623 K in a $N_2$ atmosphere.**

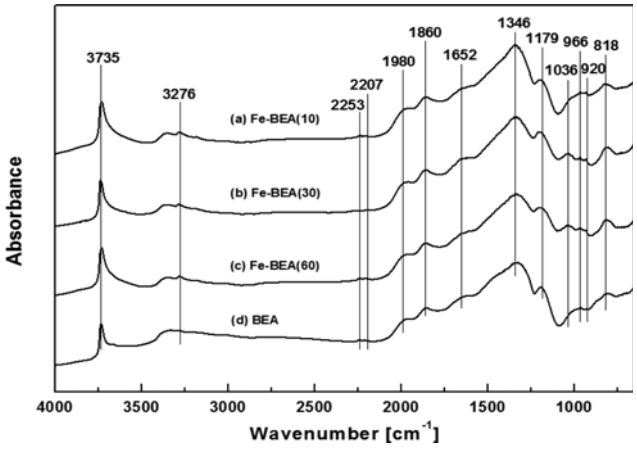


**Fig. 6. FTIR spectra of acid-treated Fe-BEA catalysts at 623 K under $NH_3$-SCR conditions.**

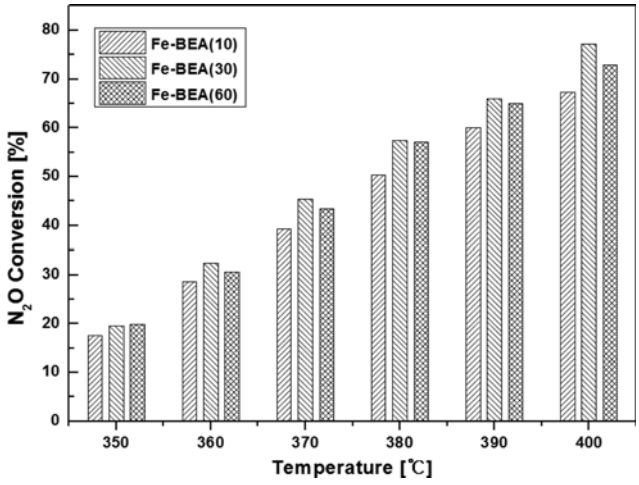


**Fig. 7. Comparison of the $N_2O$ conversion performance of Fe-BEA catalysts with different acid treatment times.**

of the band at 3, 674 $cm^{-1}$ increased and the one at 3,596 $cm^{-1}$ decreased relative to that at 3,739 $cm^{-1}$ upon Fe loading, it is reasonable to consider that the isolated bridging protons in Si(OH)Al and AlOH were exchanged with Fe species and Fe ions were bound with OH groups on catalyst surface. On the other hand, the peaks at 966 and 883 $cm^{-1}$ were associated with the oxidation state of Fe and its coordination with other atoms. The peak at 966 $cm^{-1}$ is a T-O-T framework vibration perturbed by Fe species. Therefore, the observation of this peak is evidence of successful Fe loading, and the intensity is proportional to the amount of Fe loaded. As seen in Fig. 5, the intensity of the peak at 966 $cm^{-1}$ is in the order: Fe-BEA(30)>Fe-BEA(60)>Fe-BEA(10)>BEA, that is, the most intense perturbation of T-O-T framework vibration by Fe species was observed for Fe-BEA(30). The degree of T-O-T perturbation is reported to be directly proportional to $NO_x$ desorption and conversion [40]. The peak at 813 $cm^{-1}$ was associated with stretching of Si-O-Si formed from Si-O-Al during acid treatment. This peak, which is used as an indicator of the structural stability of zeolites, was the highest in Fe-BEA(30).

Fig. 6 shows the IR spectra of the acid-treated Fe-BEA catalysts under $NH_3$-SCR conditions at a temperature of 623 K for comparison with the spectra of the Fe-BEA catalysts in a $N_2$ atmosphere (Fig. 5). Unlike the spectra in $N_2$, peaks at 3,674 and 3,596 $cm^{-1}$ were not observed in the spectra under $NH_3$-SCR conditions for any of the three samples. This result indicates that the $Fe^{III}$ species bonded to a hydroxyl group is catalytically active and is reduced to $Fe^{II}$ following reaction with $N_2O$. The peaks at 966 $cm^{-1}$ are sharper than those in the spectra in Fig. 5. Reduction of the $Fe^{III}$ species bonded to a hydroxyl group to $Fe^{II}$ would increase the degree of freedom of the Fe species and produce a stronger perturbation of the T-O-T framework vibration. Under $NH_3$-SCR conditions, the peak at 813 $cm^{-1}$ is also the most intense for Fe-BEA(30) among the Fe-BEA catalysts.

**5. Catalytic Activity Test**

Catalytic activity tests were carried out with the Fe-BEA catalysts under $NH_3$-SCR conditions. As shown in Fig. 7, the $N_2O$ conversion was found to be in the order: Fe-BEA(30)>Fe-BEA(60)> Fe-BEA(10) for all temperature ranges. These results were consistent with the behavior expected based on the analysis of the characteristics of the Fe-BEA catalysts. The increase in the number of weak acid sites produced by the acid treatment corresponded to the achievement of higher $N_2O$ conversion. This result is well matched with our assumption that the acid treatment created vacant T-sites by removing Al from the zeolite lattice and that the vacant T-sites behaved as anchoring sites for Fe ions.

## CONCLUSION

The effect of the acid treatment time on the catalytic activity of Fe-BEA zeolites for $N_2O$ conversion under $NH_3$-SCR conditions was investigated. The acid treatment did not affect physical properties of the catalyst, such as shape, size, and BET surface area. Instead, it was confirmed that tetrahedrally coordinated Al species in BEA were removed by the acid treatment and vacant T-sites were created. These vacant T-sites behaved as anchoring sites for Fe ions. The acid treatment time clearly affected the amount of weak acid sites in the Fe-BEA catalysts, as well as their catalytic activities. As the treatment time increased, the number of weak acid sites increased and the catalytic activity was enhanced. However, excessive acid treatment is believed to cause collapse of the zeolite structure, resulting in decreased catalytic activity. Therefore, with careful adjustment of the acid treatment conditions, the population of silanol groups on catalyst surface could be controlled to optimize the catalytic activity.

## ACKNOWLEDGEMENTS

This project is supported by the R&D Center for Reduction of Non-$CO_2$ Greenhouse Gases (2013001690010) funded by the Korea Ministry of Environment (MOE) as a Global Top Environment R&D Program.

## REFERENCES

1. Q. Shen, L. Li, J. Li, H. Tian and Z. Hao, *J. Hazard. Mater.*, **163**,

1332 (2009).
2. W.-H. Yang and M. H. Kim, *Korean J. Chem. Eng.*, **23**, 908 (2006).
3. J. Perez-Ramırez, F. Kapteijn, G. Mul and J. A. Moulijn, *Catal. Commun.*, **3**, 19 (2002).
4. J. P. Dacquin, C. Dujardin and P. Granger, *Catal. Today*, **137**, 390 (2008).
5. L. Obalova, K. Jiratova, F. Kovanda, K. Pacultova, Z. Lacny and Z. Mikulova, *Appl. Catal., B*, **60**, 289 (2005).
6. J. Pérez-Ramérez, F. Kapteijn, G. Mul, X. Xu and J. A. Moulijn, *Catal. Today*, **76**, 55 (2002).
7. S.-I. Tanaka, K. Yuzaki, S.-I. Ito, S. Kameoka and K. Kunimori, *J. Catal.*, **200**, 203 (2001).
8. G. Centi, L. Dall'Olio and S. Perathoner, *J. Catal.*, **192**, 224 (2000).
9. J. Pérez-Ramírez, G. Mul, F. Kapteijn, J. A. Moulijn, A. R. Overweg, A. Doménech, A. Ribera and I. W. C. E. Arends, *J. Catal.*, **207**, 113 (2002).
10. M. Galle, D. W. Agar and O. Watzenberger, *Chem. Eng. Sci.*, **56**, 1587 (2001).
11. G. Delahay, M. Mauvezin, B. Coq and S. Kieger, *J. Catal.*, **202**, 156 (2001).
12. B. Coq, M. Mauvezin, G. Delahay, J.-B. Butet and S. Kieger, *Appl. Catal., B*, **27**, 193 (2000).
13. N. Labhsetwar, M. Dhakad, R. Biniwale, T. Mitsuhashi, H. Haneda, P. S. S. Reddy, S. Bakardjieva, J. Subrt, S. Kumar, V. Kumar, P. Saiprasad and S. Rayalu, *Catal. Today*, **141**, 205 (2009).
14. C. Dai, Z. Lei, Y. Wang, R. Zhang and B. Chen, *Micropor. Mesopor. Mater.*, **167**, 254 (2013).
15. M. Kang, J. Choi, Y. T. Kim, E. D. Park, C. B. Shin, D. J. Suh and J. E. Yie, *Korean J. Chem. Eng.*, **26**, 884 (2009).
16. Y. B. Jo, J. S. Cha, J. H. Ko, M. C. Shin, S. H. Park, J.-K. Jeon, S.-S. Kim and Y.-K. Park, *Korean J. Chem. Eng.*, **28**, 106 (2011).
17. J. Yao, J. S. Choi, K. S. Yang, D. Sun and J. S. Chung, *Korean J. Chem. Eng.*, **23**, 888 (2006).
18. M. D. Gonzalez, Y. Cesteros and P. Salagre, *Micropor. Mesopor. Mater.*, **144**, 162 (2011).
19. B. Akata, J. Warzywoda and A. Sacco Jr., *J. Catal.*, **222**, 397 (2004).
20. L. Bonetto, M. A. Camblor, A. Corma and J. Perez-Pariente, *Appl. Catal., A*, **82**, 37 (1992).
21. D. Vassena, A. Kogelbauer and R. Prins, *Catal. Today*, **60**, 275 (2000).
22. M. Kogel, R. Monnig, W. Schwieger, A. Tissler and T. Turek, *J. Catal.*, **182**, 470 (1999).
23. K. Sugawara, T. Nobukawa, M. Yoshida, Y. Sato, K. Okumura, K. Tomishige and K. Kunimori, *Appl. Catal., B*, **69**, 154 (2007).
24. A. Grossale, I. Nova, E. Tronconi, D. Chatterjee and M. Weibel, *J. Catal.*, **256**, 312 (2008).
25. A. Grossale, I. Nova and E. Tronconi, *Catal. Lett.*, **130**, 525 (2009).
26. X. Zhang, Q. Shen, C. He, C. Ma, J. Cheng and Z. Hao, *Catal. Commun.*, **18**, 151 (2012).
27. M. Mauvezin, G. Delahay, F. Kiβlich, B. Coq and S. Kieger, *Catal. Lett.*, **62**, 41 (1999).
28. K. Kamasamudram, N. Currier, T. Szailer and A. Yezerets, *SAE Int. J. Fuels Lubr.*, **3**, 1664 (2010).
29. A. H. Øygarden and J. Pérez-Ramírez, *Appl. Catal., B*, **65**, 163 (2006).
30. M. Muller, G. Harvey and R. Prins, *Micropor. Mesopor. Mater.*, **34**, 135 (2000).
31. J. P. Marques, I. Gener, P. Ayrault, J. C. Bordado, J. M. Lopes, F. R. Ribeiro and M. Guisnet, *C. R. Chim.*, **8**, 399 (2005).
32. S. Moreno and G. Poncelet, *Micropor. Mater.*, **12**, 197 (1997).
33. S. Dzwigaj, P. Massiani, A. Davidson and M. Che, *J. Mol. Catal. A: Chem.*, **155**, 169 (2000).
34. R. Hajjar, Y. Millo, P. P. Man, M. Che and S. Dzwigaj, *J. Phys. Chem. C*, **112**, 20167 (2008).
35. S. M. Maier, A. Jentys and J. A. Lercher, *J. Phys. Chem. C*, **115**, 8005 (2011).
36. M. Trejda, M. Ziolek, Y. Millot, K. Chalupka, M. Che and S. Dzwigaj, *J. Catal.*, **281**, 169 (2011).
37. R. Baran, Y. Millot, T. Onfroy, J.-M. Krafft and S. Dzwigaj, *Micropor. Mesopor. Mater.*, **163**, 122 (2012).
38. J. P. Marques, I. Gener, P. Ayrault, J. C. Bordado, J. M. Lopes, F. R. Ribeiro and M. Guisnet, *Micropor. Mesopor. Mater.*, **60**, 251 (2003).
39. D. L. Bhering, A. Ramírez-Solís and C. J. A. Mota, *J. Phys. Chem. B*, **107**, 4342 (2003).
40. M. Iwasaki, K. Yamazaki, K. Banno and H. Shinjoh, *J. Catal.*, **260**, 205 (2008).